



HAL
open science

Modeling and test of a thermosyphon loop for the cooling of a megawatt-range power electronics converter

Majededdine Moustaid, Vincent Platel, Martin Guillet, Hugo Reynes, Cyril Buttay

► **To cite this version:**

Majededdine Moustaid, Vincent Platel, Martin Guillet, Hugo Reynes, Cyril Buttay. Modeling and test of a thermosyphon loop for the cooling of a megawatt-range power electronics converter. *International Journal of Thermofluids*, 2022, 13, pp.100129. 10.1016/j.ijft.2021.100129 . hal-03526803

HAL Id: hal-03526803

<https://hal.science/hal-03526803>

Submitted on 14 Jan 2022

HAL is a multi-disciplinary open access archive for the deposit and dissemination of scientific research documents, whether they are published or not. The documents may come from teaching and research institutions in France or abroad, or from public or private research centers.

L'archive ouverte pluridisciplinaire **HAL**, est destinée au dépôt et à la diffusion de documents scientifiques de niveau recherche, publiés ou non, émanant des établissements d'enseignement et de recherche français ou étrangers, des laboratoires publics ou privés.



Distributed under a Creative Commons Attribution 4.0 International License



Modeling and test of a thermosyphon loop for the cooling of a megawatt-range power electronics converter

Majededdine Moustaid^a, Vincent Platel^b, Martin Guillet^a, Hugo Reynes^a, Cyril Buttay^{c,*}

^a SuperGrid Institute, 23 rue Cyprien F-69100 Villeurbanne, France

^b Université de Pau et des Pays de l'Adour, E2S UPPA, LaTEP, Tarbes, France

^c Univ Lyon, CNRS, INSA Lyon, Université Claude Bernard Lyon 1, Ecole Centrale de Lyon, Ampère, UMR5005, 69621 Villeurbanne, France

ARTICLE INFO

Keywords:

Passive cooling
Power Electronics
Novec 649
Loop Thermosyphon

ABSTRACT

A thermosyphon loop, designed for the thermal management of a large Medium voltage power converter (5 MW overall, corresponding to a 2.4 kW thermal load per cooling unit) is presented. The device is mainly made of an evaporator, a condenser and a reservoir connected with plastic liquid and vapor lines. Novec 649 (3M) has been chosen as the working fluid due to environmental and electrical concerns. A model of the loop is described, and its predictions are compared with experiments. A first comparison yields a maximum mean deviation of 20 % between experimental results and numerical simulation at the maximum coolant temperature. The main sources of errors are identified, and improvements are proposed for better model accuracy.

1. Introduction

Recent developments in the field of power electronics, and in particular the advent of wide-bandgap semiconductor devices such as silicon carbide (SiC) [3] allow for more compact systems, and as a consequence result in denser heat fluxes. In parallel, the performance of high voltage SiC devices was found to degrade noticeably above 100 °C [4]. As a consequence, there is a need for efficient thermal management systems which can cool semiconductor chips dissipating a high power density (in the order of 100 W/cm²) down to a temperature of 100 °C or less (which, in our case, corresponds to a temperature difference ΔT of 60 °C with respect to the temperature of the environment).

Such requirements are beyond the limits of air cooling technologies. Liquid cooling (in particular using water circulation thanks to mechanical pumping) is commonly used instead, but it presents other challenges (reliability of a mechanical actuation, electrical conductivity, freezing). Passive, two-phase cooling devices are then seen as the next in line to replace air or liquid cooling systems as they offer the possibility of dissipating higher heat fluxes. Many of these systems require no pumps or moving parts as fluid circulation can rely on capillary force [5], gravity [6], electrostatic force [7] or magnetism [8]. This means that such systems can be more reliable and require less maintenance. Another advantage is that they require little to no external power to operate. Examples of such systems that have already been developed include the Capillary Pumped loop (CPL), the Loop Heat Pipe (LHP), Heat pipes (HP) and Closed Loop Thermosyphons (CLT) [9].

For our test case, hot and cold sources have to be kept apart by at least of 1 m, because of electrical isolation constraints. For the same reason, insulating pipes must be used. Furthermore, while the heat flux in the semiconductor chips can exceed 100 W/cm², these are integrated in a larger package; the actual maximum mean heat flux at the baseplate of the package is around 10 W/cm² with hot spots that can reach 15 W/cm². CLTs have shown that they can dissipate such heat fluxes, while still being easy to design, as they require no capillary structure in the evaporator nor wick structure in the pipes. Two-phase CLTs can move heat meters away with no moving parts. CLTs were thus chosen as the cooling system in the investigations presented here.

A typical CLT comprises an evaporator and a condenser. A compensation chamber can be added to replenish the evaporator with working fluid. Several CLT configurations are presented in a review article [10]. This article also includes a focus on the special needs of electronics cooling applications, but in most of the CLTs it describes are limited to a heat load of less than a few hundred watts. Another review article [11] focuses on using CLTs in data centers, which have requirements that are close to those of power electronics in terms of temperatures, heat fluxes or, in some cases, distance between evaporator and condenser [12]. One key difference, however, is the environmental conditions, which tend to be harsher for power electronics (e.g. external temperatures can drop down to -40 °C or exceed 60 °C).

CLTs can also manage more complex configurations, such as multiple heat sources: Kim et al. [13] made a CLT with two evaporators

* Corresponding author.

E-mail address: Cyril.BUTTAY@insa-lyon.fr (C. Buttay).

<https://doi.org/10.1016/j.ijtf.2021.100129>

Received 1 October 2021; Received in revised form 12 November 2021; Accepted 25 November 2021

Available online 1 January 2022

2666-2027/© 2022 The Authors. Published by Elsevier Ltd. This is an open access article under the CC BY license (<http://creativecommons.org/licenses/by/4.0/>).

Nomenclature

A	Heat exchange Area [m ²]
C_p	Heat capacity [J/(kg K)]
D	Diameter [m]
D_h	Hydraulic diameter [m]
f	Friction factor [-]
g	Gravity constant [m/s ²]
k	Singular pressure loss coefficient[]
L	Length [m]
h	Heat transfer coefficient [W/(m ² K)]
H	height [m]
$\Delta h_{\ell v}$	Latent heat of evaporation [J/kg]
L	Length [m]
M	Molar mass [kg/mol]
\dot{m}	Mass flow rate across the interface [kg/s]
p	Pressure [Pa]
p_r	Reduced pressure [Pa]
\dot{Q}	Heat dissipation [W]
q	heat flux [W/m ²]
R	Roughness [μm]
Re	Reynolds number [-]
S	Cross section [m ²]
t	Time [s]
T	Temperature [K]
V_v	Vapor volume [m ³]
v	Velocity [m/s]

Greek characters

ρ	Fluid density [kg/m ³]
μ	Dynamic viscosity [Pa.s]
λ	Thermal conductivity [W/(m K)]

Subscripts

0	relative height from the ground
A	ambient
$boil$	Boiling
$block$	Heating block mounted onto the evaporator
c	Baseplate
C	Condenser
$Cooper$	Boiling formula from [1]
ext	External
exp	Experimental
E	Evaporator
f	Fluid
in	Inlet
int	Internal
$Louahlia$	Boiling formula from [2]
ℓ	Liquid
out	Outlet
r	Reduced

R	Reservoir
sat	Saturation
SS	Stainless Steel
T	Tube
v	Vapor
w	Water

CLT with two different arrangements and was able to achieve a cooling of 70 W/cm² with a heat load of up to 1300 W. Such high heat flux was permitted by adding a capillary structure at the evaporator. In their conclusions, the authors recommend such a system over heat pipe assemblies for flexibility and performance reasons. To manage even higher heat fluxes, Hartenstine et al. [15] studied different wick structures in the evaporator of a CLT for naval electronic applications. With a bi-porous wick structure, they reached a heat flux of 465 W/cm², using copper/water couple with sub-atmospheric operating conditions ($T_{sat} = 70^\circ\text{C}$). Regarding higher power levels, Agostini et al. [16] made a CLT to cool down power electronics; R245fa was chosen as the coolant with a water-cooled condenser; a flexible metallic vapor line and a flexible plastic (PVFD) liquid line were implemented for ease of placement and maneuver. The authors were able to dissipate between 5 and 12.5 kW in the evaporator. The authors also completed their experimental work with a numerical model that had a maximum deviation of 26% between the measured and the calculated thermal resistance.

However, most fluids have detrimental effects on the environment such as toxicity and ozone depletion power, or present safety issues such as flammability (more details are given in Section 2.1). In [17], the authors present a CLT based on R134a, a refrigerant which addresses these issues, but offers poor thermal performance. As a result, heat fluxes at the evaporator are found to be limited to 2.8 W/cm². Furthermore, the high global warming potential of R134a (1300 times that of CO₂) has recently made it less attractive from an environmental point-of-view.

In this paper, we present a two-phase CLT dedicated to a large power electronic converter (2400 W max. heat dissipation). The instrumented, full scale prototype which was build to analyze its operation is presented in Section 2. The working fluid is Novec 649, a choice was made considering the health, environmental, practical and electrical aspects, in addition to pure thermal performance [18]. To the best of our knowledge, this is the first full-scale thermosyphon implementation using this particular fluid. In addition to presenting experimental results, we also describe a theoretical model (Section 3) based on coupling heat, mass, and momentum equations, in the different volumes of the loop. This model can be used to calculate the temperature, pressure and flow at different points of the loop. These calculations are compared with the experimental data in Section 4. Finally, the results are discussed, and improvements are proposed for the model, as well as for the thermosyphon loop.

2. Experimental device

The experimental setup is presented in Fig. 1. Its main components are an evaporator, a condenser and a reservoir, connected with plastic tubing. In operation, heat is dissipated from the heating blocks attached to the evaporator, causing the fluid to boil. The newly formed vapor then rises from the evaporator to the condenser, where it returns to its liquid state after releasing some of its heat into the water. The liquid condensate returns to the reservoir then to the evaporator, completing the loop.

All the components of the CLT are connected through plastic flexible hose (Thermoclean 100, a PVC multilayer tube that can withstand up to 5 bar at 100 °C), to allow for easy re-positioning of the components.

(up to 650 W each). However, it was found that an unbalance in heat dissipation as small as 5% between the evaporators produced dry patches in the one with the highest heat input. This was associated with an unbalance in temperature, pressure and flow patterns in the loop.

A variety of fluids has been investigated for CLT applications over the years [10]. Krushtalev [14] studied the capabilities of a methanol

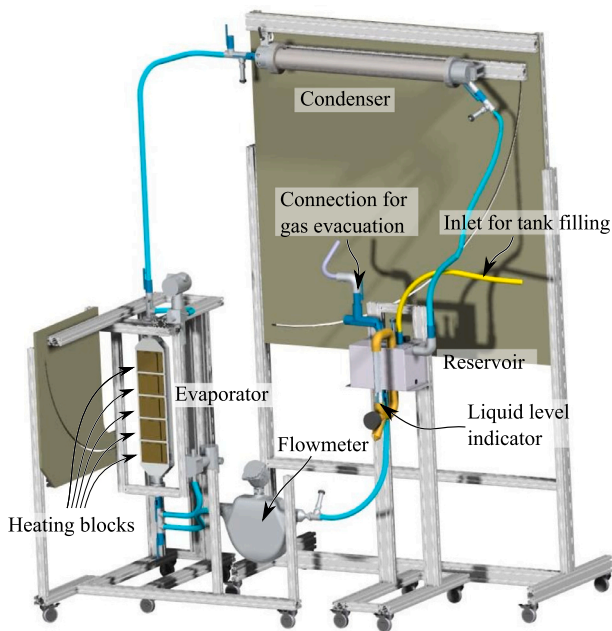


Fig. 1. 3D model of the actual closed-loop thermosyphon test bench. Overall dimensions are $\approx 3 \times 2$ m. Evaporator and Condenser can be tilted at different angles, from vertical to horizontal here, the evaporator is represented in the vertical orientation (90°) and the condenser is horizontal (0°). Note that the elements (evaporator, condenser, reservoir, and the sensors) are actually connected together using flexible hose with different lengths than represented here.

Table 1
List of constraints and values of the parameters impacting the fluid choice.

Constraints	Parameter	Acceptable values
Ozone effect	ODP	0
Greenhouse effect	GWP (PRG)	<150
Flammability	HMIS(ou NFPA)	0
Toxicity	HMIS(ou NFPA)	0
Stability	HMIS(ou NFPA)	0
Electric	Resistivity	$>9 \times 10^5 \Omega\text{m}$

2.1. Cooling fluid

Project specifications made it so that usual coolants were not a viable option for such a project. These constraints focused on environmental, safety and thermal aspects and can be summarized in [Table 1](#).

To find the appropriate candidate, 40 fluids were investigated ([Fig. 2](#)). Out of these fluids, Novec 649 (3M) comes on top. From an environmental point of view, it has an Ozone Depletion Power (ODP) of 0 and a Global Warming Potential (GWP, expressed in CO_2 equivalents) of 1. Regarding health and safety, it is not flammable, and has low toxicity. Finally, it is an electric insulator, which allows evaporator and condenser to be at different electrical potentials (a desirable feature for medium voltage converters, where the voltage difference can be of tens of kilovolts).

Its thermodynamic properties, summarized in [Table 2](#), indicate low thermal performance compared to common fluids (and in particular to water). This is also confirmed by comparing its thermosyphon figure of merit [9]:

$$M = \left(\frac{\lambda_\ell^3 \Delta h_{\ell v} \rho_\ell}{\mu_\ell} \right)^{0.25} \quad (1)$$

The values of this figure of merit ([Fig. 2](#)) suggest that water is by far the best fluid. In addition, water does not present any environmental challenge. However, it is unsuitable to low temperatures ($< -40^\circ\text{C}$

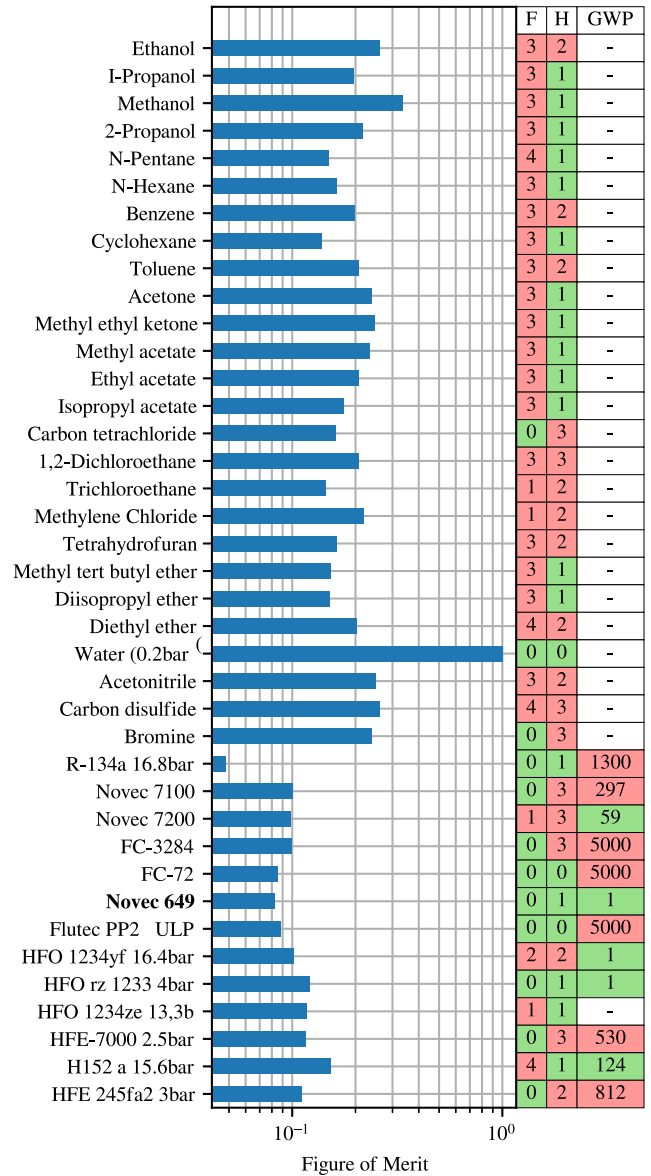


Fig. 2. Review of possible cooling fluids, considering their thermal performance (figure of merit) in a CLT, their flammability (F), health issues (H), and global warming potential (GWP, as compared to CO_2).

Table 2
Thermodynamic properties of Novec 649 [19].

Boiling temperature (1 bar)	49 °C
Liquid density ρ_ℓ	1600 kg/m ³
Vapor density ρ_v	5.73 kg/m ³
Liquid viscosity μ_ℓ	0.64 mPa/s
Latent heat $\Delta h_{\ell v}$	88 kJ/kg
Thermal conductivity λ_ℓ	0.059 W/(mK)
Surface tension	10.8 mN/m
Molar mass	316.04 g/mol
Melting temperature	-108 °C

in our case), and require special precautions to remain electrically insulating.

Novec 649 can operate over a large temperature range, and is also of low environmental concern, but it is expected to exhibit only modest performance in a CLT. This may explain why only a few research articles have been published so far where Novec 649 is used as a cooling fluid. Among them, the authors of [20] investigate the cooling of a hot

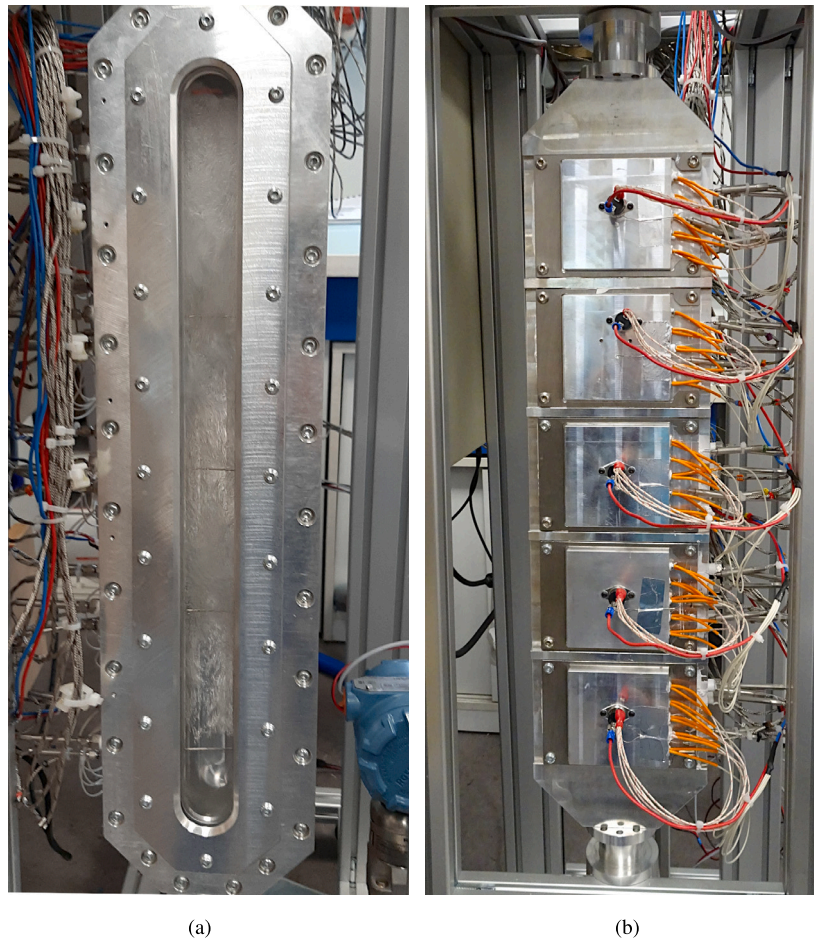


Fig. 3. Photographs of the evaporator: (a) Sight glass showing the fluid in boiling mode; (b) back of the evaporator showing the five heating blocks with their respective wiring (heating cartridges, thermocouples).

wire submerged in a pool of 649, and demonstrate that heat transfer is comparable to that of FC72, a popular cooling fluid with a very high GWP (more than 5000, with a very long atmospheric lifetime). In [21], the authors use Novec 649 in a pulsating heatpipe, achieving an equivalent thermal conductivity from evaporator to condenser of almost 5000 W/(mK), or 12.5 times that of pure copper. Finally, a paper from Agostini et al. [22] seems to constitute the first report of a Novec-649 thermosyphon. The device it describes, however, is more suited to lab investigations than to an actual cooling application, and the paper itself focuses on metrology issues (the measurement of mass-flowrate in the case of liquid entrainment in the vapor line).

2.2. Evaporator

The evaporator is a large aluminum (6061 T6) part ($66.5 \times 16 \times 4 \text{ cm}^3$) with smooth internal surfaces (Fig. 3). One side permits to glance via a rectangular sight glass (PERSPEX® “Glass Look”, 10 mm-thick) at the dynamics and boiling processes inside the evaporator filled with the working fluid as shown in Fig. 3(a). The back of the evaporator is shown in Fig. 3(b), with five heating blocks attached to it (thermal grease is applied at the interface between the blocks and the evaporator, and the evaporator wall thickness on the block side is 5.5 mm). These aluminum (6061 T6) blocks emulate the thermal behavior of power electronic modules (contact surface of each block: $10 \times 14 \text{ cm}^2$). Each heating block can dissipate up to 1100 W thanks to 5 heat cartridges (TC direct model 921-124, diameter 6.5 mm). Eurotherm E-Pack controllers are connected to each block, allowing a precise control of the dissipated power, regardless of possible variations

in the resistance of the heat cartridges. Thermocouples are used to measure the temperature at different locations (fluid, heat exchanger wall, heating blocks).

2.3. Condenser

The condenser is a custom, countercurrent, multi-tubular heat exchanger entirely made out of stainless steel (Fig. 4). It was designed to dissipate the nominal power with a temperature difference $\Delta T < 10 \text{ }^\circ\text{C}$ between the incoming saturated vapor and the maximum cooling water temperature (set at 25 or 40 $^\circ\text{C}$). Water coolant temperature and flow-rate can be controlled by a chiller (Julabo FL4003) that is connected to the condenser.

Both the evaporator and the condenser can be tilted between the vertical and horizontal position at any chosen angle. In this study, the evaporator was tilted at an angle of 75° while the condenser angle was fixed at an angle of 15° with respect to the horizontal.

2.4. Reservoir

A reservoir ($30 \times 20 \times 20.4 \text{ cm}^3$, stainless steel) is implemented between the condenser and the evaporator. It protects the condenser from flooding when operating at high power level and high filling ratios. The reservoir also regulates fluid supply to the evaporator to prevent it from drying out. The position (height) of the reservoir can be adjusted to control the filling ratio of the evaporator. In this study, the reservoir is at its maximum height. This means that, at rest, the evaporator is totally filled with liquid.

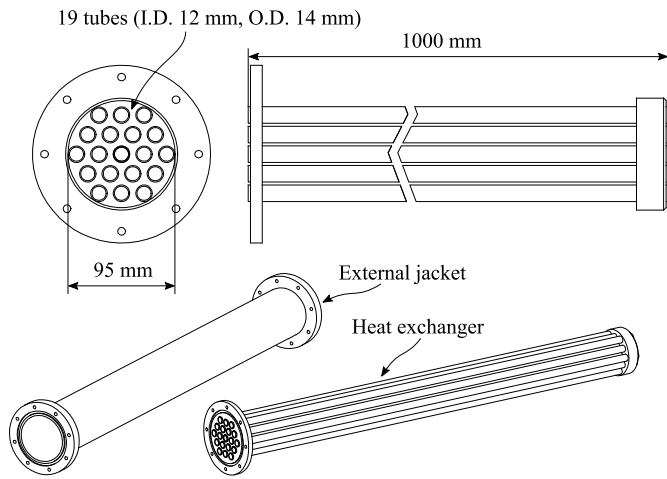


Fig. 4. Details of the internal structure of the condenser, and 3D views of the tube heat exchanger and its external jacket. The end caps, which receive the connections, are not represented for the sake of clarity.

2.5. Instrumentation

Many sensors have been integrated to monitor the CLT operation (see Fig. 5 for position). Overall, 37 T-type thermocouples are used for temperature measurements: in the evaporator, 15 thermocouples measure the fluid temperature in various places, 10 the wall temperature (2 under each of the 5 heating blocks) and 5 are located on top of the heating blocks; the condenser is equipped with 2 thermocouples (one at each end); 2 thermocouples are placed in the reservoir, one in the vapor and one in the liquid region; 2 thermocouples are placed in the water cooling circuit, one at the inlet and one at the outlet of the condenser; finally, one last thermocouple measures the ambient temperature. The thermocouples in contact with the fluid are 1.5 mm in diameter while those attached to the heating blocks are 0.5 mm in diameter.

Pressure sensors are located at both ends of the evaporator (Rosemount model 3051S1CD), in the liquid line, in the vapor region of the reservoir, and at both ends of the condenser (Keller Model 33X). Finally a Coriolis-type flowmeter (Emerson model CMFS075M) is placed in the liquid line while another flowmeter (GPI model A 100) is placed in the cooling water circuitry.

2.6. Connection of the parts

All the components of the CLT are connected through flexible PVC hoses (Tricoflex® Thermoclean® 100) to allow for easy re-positioning of the components. To simplify the design, the same hoses (internal diameter: 25 mm, external diameter: 35 mm) are used for both the vapor and liquid lines. Note that because electrical isolation is needed between the various parts of the loop, the selected hoses do not contain any metallic reinforcement. As a consequence, these hoses, which can withstand a pressure of more than 6 bar and a maximal temperature of 100 °C, tend to flatten under negative pressure (this is not a problem here, as the CLT does not normally operate below atmospheric pressure).

The hose lengths are 2.15 m between evaporator and condenser, 1.5 m between condenser and reservoir, and 4.6 m between reservoir and evaporator. Stainless steel fittings are standard BSPT 1 in, using FKM (Viton) seals. The chemical compatibility of seals and hoses with Novec 649 was tested beforehand by leaving samples of these materials to soak in Novec for 24 h at 70 °C (using a pressure vessel SR-TEK 3800ML-LT) and measuring negligible change in weight ($\leq 0.05\%$).

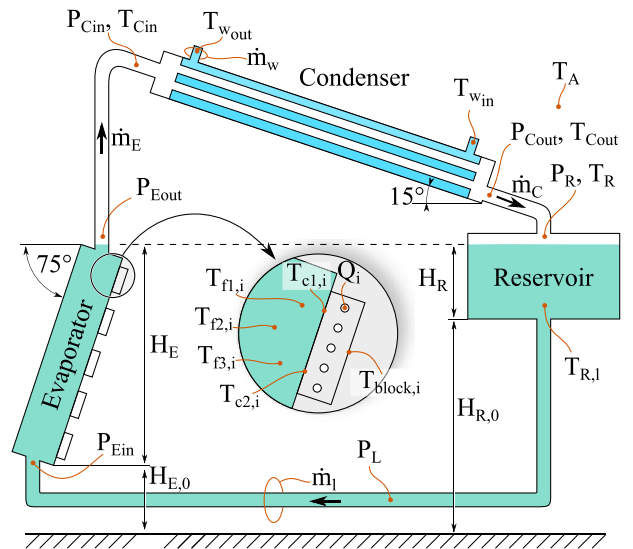


Fig. 5. 2D sketch of the thermosyphon with the parameters that are monitored in the experiment (orange lines). Note that the drawing is not to scale. (For interpretation of the references to color in this figure legend, the reader is referred to the web version of this article.)

3. Model

Fig. 5 shows the variables to be calculated, which requires coupling fluid and thermal equations. For that purpose, the thermosyphon is divided into five main elements: heating blocks, evaporator, condenser, reservoir and liquid line.

The heat equation is used to calculate the temperature distribution across the loop, while mass and momentum are used for the mass flow and pressure distribution.

Starting with the mass conservation, the equations can be written as (a nomenclature is provided at the end of the article):

$$\frac{dH_E}{dt} = \frac{\dot{m}_\ell - \dot{m}_E}{\rho_\ell A_{E,\ell}} \quad (2)$$

$$\frac{dH_R}{dt} = \frac{\dot{m}_C - \dot{m}_\ell}{\rho_\ell A_{R,\ell}} \quad (3)$$

where H_E and H_R refers to the height of the evaporator and the reservoir; $\dot{m}_\ell, \dot{m}_E, \dot{m}_C$ to the mass flow rate of the liquid, through the evaporator and through the condenser; ρ_ℓ to the density of the liquid phase; $A_{E,\ell}$ and $A_{R,\ell}$ to the heat exchange surface in contact with liquid in the evaporator and reservoir, respectively. To calculate the liquid flow inside the loop, we use momentum conservation equations for the evaporator, the reservoir and the liquid line (Viscous pressure drop in the vapor phase are neglected) :

$$\rho_\ell A_{E,\ell} \left(v_{E\ell} \frac{\dot{m}_\ell - \dot{m}_E}{\rho_\ell A_{E,\ell}} + H_E \frac{dv_{E\ell}}{dt} \right) = v_{E\ell} (\dot{m}_\ell - \dot{m}_E) - \rho_\ell g A_{E,\ell} H_E + A_{E,\ell} (p_{E,in} - p_{E,sat}) \quad (4)$$

$$\rho_\ell A_{R,\ell} \left(v_{R\ell} \frac{\dot{m}_R - \dot{m}_\ell}{\rho_\ell A_{R,\ell}} + H_R \frac{dv_{R\ell}}{dt} \right) = v_{R\ell} (\dot{m}_R - \dot{m}_\ell) + \rho_\ell g A_{R,\ell} H_R + A_{R,\ell} (-p_{R,out} + p_{R,sat}) \quad (5)$$

$$\frac{d\dot{m}_\ell}{dt} = A_{C,\ell} \frac{\rho_\ell g (H_{R,0} - H_{E,0}) + p_{R,out} - p_{E,in} - \Delta P_{ch,L\ell}}{L_\ell} \quad (6)$$

with v the velocity, g the gravity constant, p the pressure and L_ℓ the length of the liquid line. Combining Eqs. (4)–(6) gives the liquid flow rate \dot{m}_ℓ :

$$\frac{d\dot{m}_\ell}{dt} \left(\frac{L_\ell}{A_{C,\ell}} + \frac{H_R}{A_{R,\ell}} + \frac{H_E}{A_{E,\ell}} \right) = \rho_\ell g (H_{R,0} + H_R - H_{E,0} - H_E) + p_{R,sat} - p_{E,sat} - \Delta P_{ch,L\ell} \quad (7)$$

The pressure drop in the liquid line is calculated as a sum of the linear and the singular losses:

$$\Delta p_{cHL} = f \frac{4\rho_\ell v_\ell^2 L_\ell}{2D_h} + \sum k \left(\frac{\rho_\ell v_\ell^2}{2} \right) = \frac{\dot{m}_\ell^2 \left(4f \frac{L_\ell}{D_h} + \sum k \right)}{2\rho_\ell S^2} \quad (8)$$

where D_h is the hydraulic diameter and S the cross section of the line. The friction coefficient f is calculated depending on the flow nature [23] using Reynold's number Re :

$$f = \begin{cases} 1 & \text{for } Re_\ell < 1 \\ \frac{16}{Re_\ell} & \text{for } 1 \leq Re_\ell \leq 2000 \\ 0.079 Re_\ell^{-0.25} & \text{for } Re_\ell > 2000 \end{cases} \quad (9)$$

As for the singular pressure loss, the coefficient k is calculated assuming a simple law of surface sudden variation.

The vapor flow rate in the vapor line is calculated from the vapor generation due to boiling at steady state:

$$\dot{m}_E = \frac{h_{boil} \sum_1^5 A_{c,i} (T_{c,i} - T_{f,sat})}{\Delta h_{\ell v}} \quad (10)$$

With T denoting a temperature and h a heat exchange coefficient. Fluid displacement is associated with a pressure loss. Since vapor pressure travels at the speed of sound and we can assume that there is no inertia associated with vapor movement, we can associate all pressure loss to friction. Pressure loss in the vapor line is therefore calculated using (8), with the friction coefficient calculated by substituting the vapor Reynolds number (Re_V) to its liquid counterpart (Re_ℓ) in (9).

Moving on to temperature calculations, there are 5 identical and independent heating blocks mounted on the evaporator. We are interested here in calculating only the wall temperature of the blocks, assuming a uniform surface distribution. Each wall temperature on the block i can be calculated as follows :

$$m_{block} C_{p,alu} \frac{dT_{c,i}}{dt} = \dot{Q}_i - h_{f,i} A_{f,i} (T_{c,i} - T_{f,sat}) - h_{A,i} A_{A,i} (T_{c,i} - T_A) \quad (11)$$

With C_p the heat capacity of the corresponding material and \dot{Q}_i the heat dissipation of block i . The model of the condenser has already been published in a previous communication [24]. Unlike the rest of the loop, the condenser is modeled in static conditions making a hypothesis of instant condensation of the vapor.

Cavallini's model [25] is used to predict the condensation heat exchange coefficient. The condensed mass flow rate can be calculated as the following (x being a vapor mass fraction):

$$\dot{Q}_C = \frac{(T_f - T_w)}{R_{th}} = (x_{in} - x_{out}) \dot{m}_C \Delta h_{\ell v} = \dot{m}_w C_{p\ell w} \Delta T_w \quad (12)$$

R_{th} is the condenser thermal resistance, calculated as:

$$R_{th} = \frac{1}{h_{cond} A_{int}} + \frac{\ln \left(\frac{D_{ext}}{D_{int}} \right)}{2\pi \lambda_{SS} L} + \frac{1}{h_w A_{ext}} \quad (13)$$

Where λ_{SS} is the thermal conductivity of stainless steel, the material of the condenser. Vapor density in the vapor line and the condenser is calculated based on a mass balance equation. It is expressed as follows V_V being the vapor volume:

$$\frac{d\rho_v}{dt} = \frac{(\dot{m}_E - \dot{m}_C)}{V_v} \quad (14)$$

3.1. Heat exchange coefficient in the evaporator

Boiling heat transfer is complex, as it simultaneously involves multiple mechanisms [26]. Some mechanistic models have been developed over the years to predict boiling heat transfers. However, they are difficult to implement as they require a deep knowledge of many parameters such as bubble diameters, bubble frequency and the number of nucleation sites. These parameters are not always known, since they

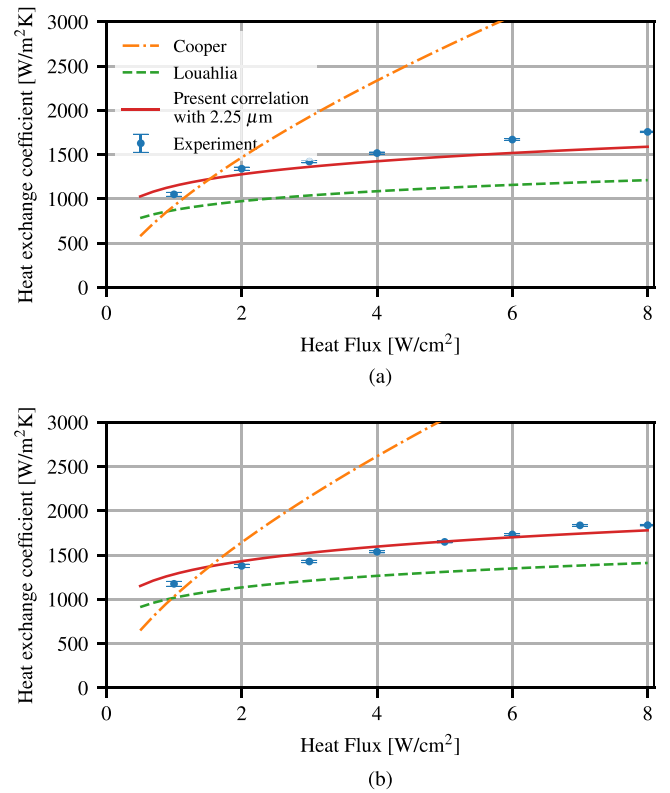


Fig. 6. Comparison of the heat exchange predictions of various correlations with the experimental values, for water chiller temperature of 25 °C (a) and 40 °C (b).

highly depend on the geometry and the wall surface condition. An alternative is to use heat transfer correlations. These empirical equations provide a satisfying prediction of the average heat transfer, while only requiring fluid and surface properties which can be found easily. A large number of correlations has been proposed over the years [26]. Nevertheless, few such correlations exist when operating under sub-atmospheric pressure. One was proposed by Louahlia-Gualous et al. [2]. The formula was derived from the classic Cooper's heat exchange correlation [1] to fit experimental data:

$$h_{E,Cooper} = 55M^{-0.5} q^{0.67} \frac{p_r^{0.12-0.2 \log_{10} R}}{-\log_{10} p_r} \quad (15)$$

M being the molar mass of the fluid, and q the heat flux through the surface. Cooper's formula takes the roughness R of the boiling surface into account. As R is rarely known, Louahlia's derived correlation considered an arbitrary, fixed value for R :

$$h_{E,Louahlia} = 7704M^{-0.5} q^{0.157} \frac{p_r^{0.12}}{-\log_{10} p_r} \quad (16)$$

For our evaporator, R is estimated by the manufacturer to be in range of [2 μ m; 4 μ m]. Considering $R = 2.25 \mu m$, Louahlia's equation becomes:

$$h_{E,this_work} = 7704M^{-0.5} q^{0.157} \frac{p_r^{0.12-0.2 \log_{10} R}}{-\log_{10} p_r} \quad (17)$$

This adjusted equation yields a better correlation with the experimental results (less than 11 % error) as shown in Fig. 6. The experimental heat exchange coefficient is calculated at steady state (see next section for the experimental protocol) as:

$$h_{E,exp} = \frac{\dot{Q}_{block,3}}{(T_{c,3} - T_{f,3}) A_{block,3}} \quad (18)$$

Table 3
Model parameters.

Reservoir		Evaporator		Condenser		Piping		Heating block	
H_R	0.2 m	H_E	0.6 m	D_{int}	12 mm	R_T	20 mm	A_{block}	10 cm ²
H_{RO}	1.2 m	H_{EO}	0.65 m	D_{ext}	14 mm	L_f	6.1 m	H_{block}	13 mm
A_R	0.06 m ²	A_E	0.004 m ²	\dot{Q}_W	35.5 L/min	L_v	2.15 m		
		λ_E	121 W/(m K)	λ_C	16 W/(m K)				
		R	2.25 μ m	Nc	19				
				L_C	1 m				

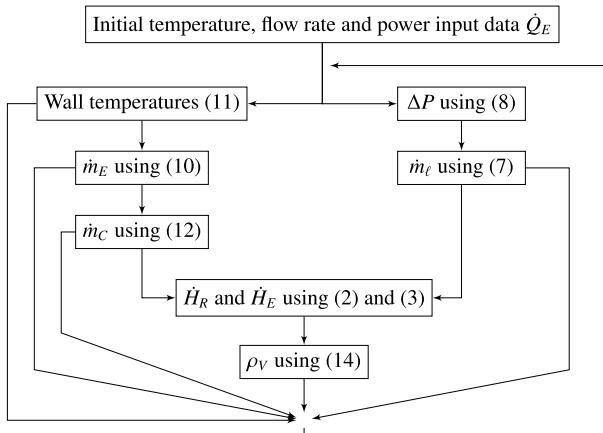


Fig. 7. Algorithm for the implementation of the CLT model.

Table 4

Main parameters of the thermosyphon loop.

	Parameters	Interval
Heating block	Power	300 to 2400 W
Evaporator	Inclination angle	75°
Condenser	Inclination angle	15°
Chiller	Temperature	25 °C, 40 °C
	Volum. flow	35.5 L/min

With $Q_{block,3}$ the power dissipated by the middle heating block (#3, so no heat spreading effect has to be considered), $T_{c,3}$ is the wall temperature (the average of $T_{c1,i}$ and $T_{c2,i}$ in Fig. 5), $T_{f,3}$ the temperature of the fluid (average of the 3 temperature measurements $T_{f1,i}$, $T_{f2,i}$ and $T_{f2,i}$ in Fig. 5) and $A_{block,3}$ the area of the exchange surface between block 3 and the fluid (100×140 mm).

Fig. 7 describes the algorithm used to couple and solve these equations using a python script, with a time step of 0.01 s. Water and Novec 649 properties as a function of the temperature were taken from the NIST REFPROP 10.0 fluid database. Model parameters are shown in Table 3.

4. Experimental analysis and numerical comparison

4.1. Experimental protocol

The filling protocol is as follows: first, the loop is evacuated using a vacuum pump connected to the reservoir (Fig. 1). Once evacuated down to a pressure of less than 1 kPa, the reservoir is connected to a tank containing the Novec 649 which has previously undergone evaporation/condensation cycles to remove any non-condensable gas.

The temperature and pressure measurement in the vapour phase of the reservoir makes it possible to know the quantity of non-condensable gas produced, as they accumulate over time in this element of the loop. At the beginning of each test series (typically every morning), these non-condensable gas are evacuated using the vacuum pump.

In the following, the effects of two parameters are investigated. The first parameter is the temperature of the water coming out of the chiller

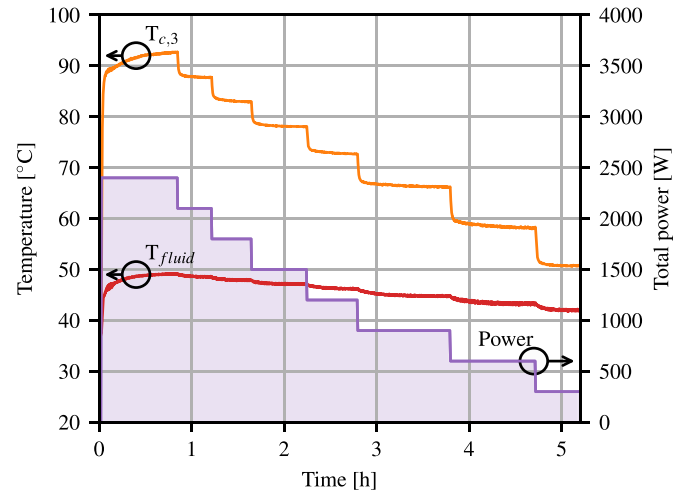


Fig. 8. Example of some temperatures recorded during a typical test of the CLT: power is injected in decreasing amount (from 2400 down to 300 W, with steps large enough to reach steady state. This graph shows that the CLT exhibit a stable behavior, with no oscillations and rapid adaptation to power variations.

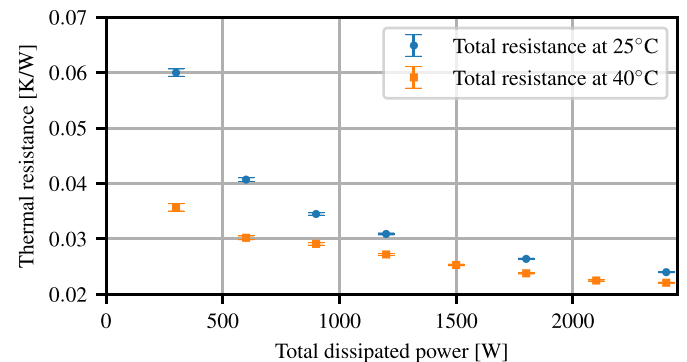


Fig. 9. Thermal resistance of the CLT as a function of the power dissipated by the heating blocks, for two temperatures of the cooling water.

(25 °C or 40 °C). The second is the total heat flux dissipated by the heating blocks (from 2400 W down to 300 W). For each configuration, enough time is allowed for the loop to reach steady-state (\approx 30 min). An example of the data recorded during the operation of the CLT is given in Fig. 8. In the rest of the article, the dynamic behavior is not considered, and all data will correspond to steady-state values.

All the other parameters of the loop are kept constant, and are summarized in Table 4. The main criterion for the comparison between simulation and experiment is the thermal resistance of the CLT, as it is the main metric for power electronics applications.

4.2. Measurement of the thermal resistance of the CLT

From a global perspective, Fig. 9 shows the evolution of the CLT total thermal resistance, calculated as the sum of three main resistances

(evaporator, condenser and the tube connecting them referred to as riser):

$$R_{tot} = \underbrace{\frac{T_c - T_{C,w,mean}}{\dot{Q}}}_{\text{total resistance}} = \underbrace{\frac{T_c - T_{E,f}}{\dot{Q}}}_{\text{evaporator}} + \underbrace{\frac{T_{E,f} - T_{C,f,in}}{\dot{Q}}}_{\text{riser}} + \underbrace{\frac{T_{C,f,in} - T_{C,w,mean}}{\dot{Q}}}_{\text{condenser}} \quad (19)$$

where T_c represents the maximum temperature measured at the evaporator wall, $T_{E,f}$ is the fluid saturation temperature measured in the fluid inside the evaporator, $T_{C,f,in}$ is the condenser inlet temperature and $T_{C,w,mean}$ is the mean water coolant temperature. The heat flux \dot{Q} through the evaporator, riser and condenser is considered constant, i.e. we consider there is no heat “leakage” to the environment. The consequences of this strong assumption are discussed further below.

The drop in thermal resistance value as power increases (Fig. 9) can be attributed to the increase in boiling and condensation heat transfer coefficient with the heat flux.

It can also be noted that a lower water temperature results in a larger thermal resistance. This can be explained by two key factors. First, the vapor density is proportional to the saturation temperature; the lower vapor density observed at a lower temperature results in higher vapor velocity and higher vapor fraction inside the evaporator; this increases pressure losses and reduces liquid replenishment, making it easier to form dry spots. The second factor is the occurrence of heat losses over the entire CLT despite the insulation of both the reservoir and the condenser. This was confirmed by comparing the power injected at the heat blocks and that collected by the water flow at the condenser: while this difference is negligible (a few percents) when operating with a 25 °C water temperature (i.e. close to the temperature of the air surrounding the CLT), it becomes much larger (more than 10%) for 40 °C. For the smallest power levels (300 W), this difference may even reach 50%, meaning that half of the power is lost to the environment before reaching the condenser.

Fig. 10 represents the values of the elementary thermal resistances from (19) and their contribution to the total thermal resistance of the CLT. It can be noted that the evaporator accounts for the main share in the total thermal resistance (up to 80%). This can be explained by a combination of thermophysical properties of the fluid such as wetting and by the smoothness of the flat heat exchange surface. Possible improvements are discussed in Section 4.4.

4.3. Comparison of simulated and measured thermal resistances

Fig. 11 presents a comparison between the wall temperatures calculated using the correlations from Section 3.1 and the measured data, for both cooling water temperatures. It confirms that the proposed correlation fits the experimental data the best, especially for the higher power levels, which is the most important case in our thermal design.

Fig. 12 presents a comparison of the overall thermal resistance between experimental and numerical results calculated using the correlation proposed here. It shows that the total resistance is predicted within a maximum of 20% of error for power levels of more than 600 W.

Finally, Fig. 13 illustrates a comparison between the experimental and numerical volume flow rate as a function of dissipated power. We can notice that the model’s accuracy increases with the power injected in the loop. One of the reasons that could explain differences between the measured and the calculated values is the presence, unaccounted for in the model, of liquid in the vapor line: some liquid is pushed by the vapor and travels to the condenser at high powers levels, and some vapor condensates in the riser and flow back to the evaporator before reaching the condenser. A complete review of correlations for liquid/vapor interactions in the riser is proposed in [27]. Note that Fig. 13 was limited to powers higher than (>1200 W), as liquid flow became intermittent for lower power. Comparison at lower power levels would be erroneous, as we assumed a continuous flow for the model.

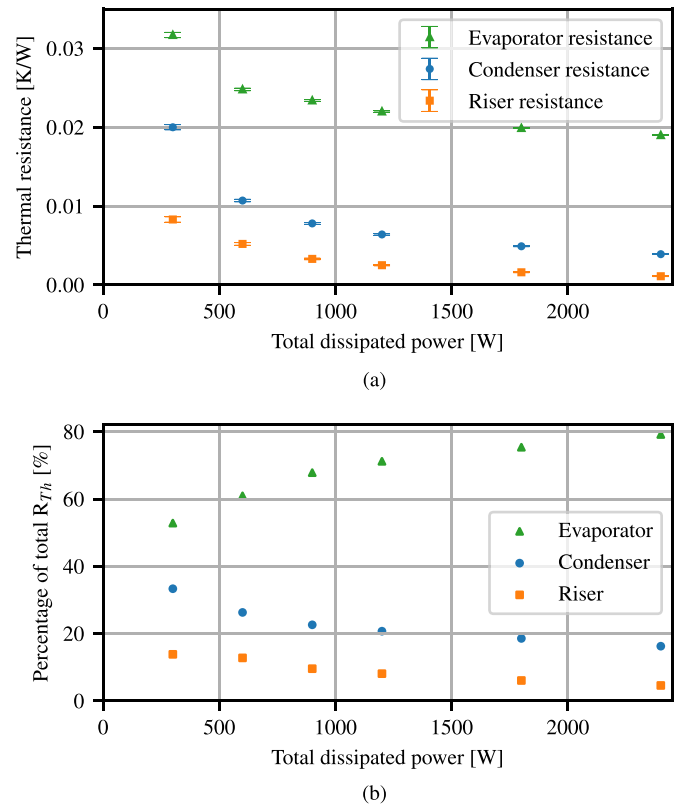


Fig. 10. Contribution of the evaporator, the riser tube and the condenser to the thermal resistance Resistance. Absolute values (a) and percentage of the total thermal resistance (b). Water chiller temperature is 25 °C.

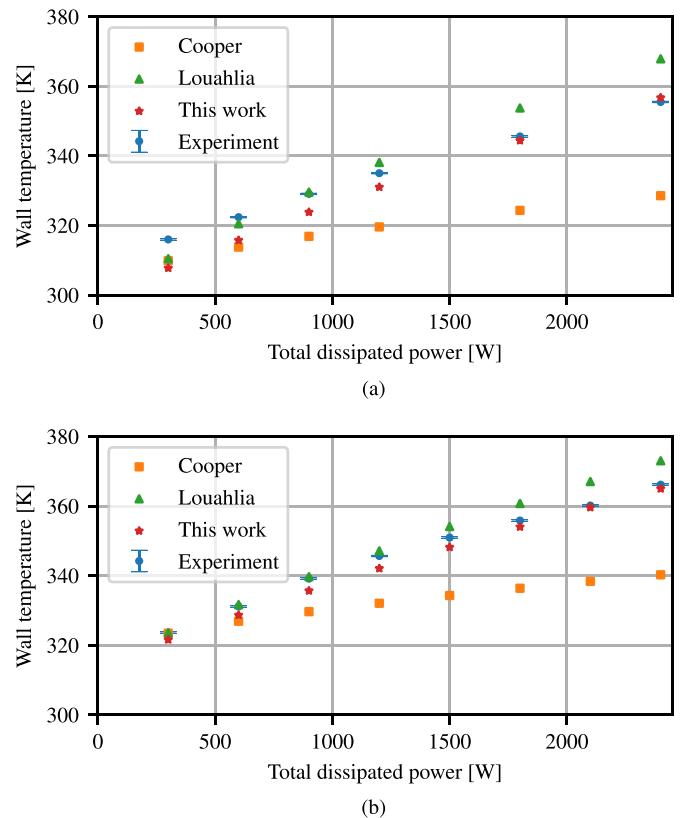


Fig. 11. Wall temperature as calculated with the three correlations from (15)–(17) and acquired experimentally, for (a) 25 °C water temperature and (b) 40 °C water temperature.

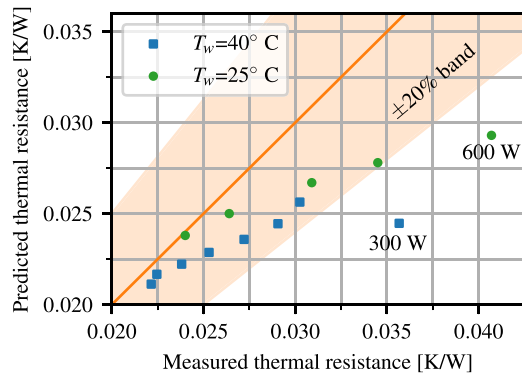


Fig. 12. Predicted and measured values of the loop thermal resistance, for water chiller temperatures of 25 and 40 °C. Datapoints measured for low power levels (300 W for $T_w = 40$ °C and < 600 W for $T_w = 25$ °C) exhibit deviation of more than 20% with the predicted value.

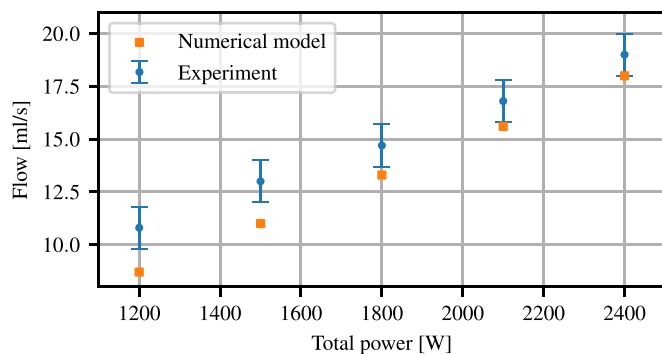


Fig. 13. Mass flow rate comparison between the numerical values and the experimental measurements, water chiller temperature is 40 °C.

4.4. Improvements to the model and the test setup

This model already gives an acceptable approximation of the experimental results, especially for the higher power levels. Its accuracy can be improved further by taking into account the sub-cooling phenomena in the loop. The liquid flow passes through many metallic connections from the condenser until it reaches the evaporator, heat loss is noticeable and should be included in any future model. This can be done by adding a thermal model that can calculate heat exchange in the metallic connections and the liquid line but also the condensation in the vapor line.

Another area of enhancement would be the implementation of a dynamic model to simulate flow instabilities. Early experimental observations show the possibility of flow oscillation that affect the operating parameters of the entire loop (temperature, pressure and flow). These oscillations, caused by two-phase flow instabilities, have been empirically dampened by constricting the liquid flow at the evaporator inlet with valve throttling. Predicting such instabilities is crucial for the design of industrial-grade thermosyphons.

Regarding the experimental setup itself, some performance improvements can also be proposed. As presented in Fig. 10(a), the main contributor to the overall thermal resistance is the evaporator. Its smooth boiling surface should be replaced by a rough and patterned surface (pins, fins, corrugations, etc.). This would lead to increasing both boiling surface and nucleation sites number, resulted in a much higher exchange coefficient and a reduced thermal resistance. The geometrical aspect of surface patterns is a parameter to be optimized in any future study. However, it is worth noting that in its current configuration, the CLT is already able to meet the requirements of the application.

5. Conclusion

In the present study, a closed loop thermosyphon is used to study the heat exchange capabilities of Novec 649 under a power load reaching 2.4 kW. Experimental results show that boiling represents the main contribution to the thermal resistance ($\approx 80\%$ at high power dissipation), although this could largely be reduced by modifying the boiling surface.

A simple model is presented, which couples heat, mass and momentum equations. Because of the very large contribution of the boiling phenomenon to the overall thermal resistance, existing correlations are adjusted to offer a more accurate estimation of the heat exchange coefficient at the boiling surface. Overall, the proposed model is found to predict thermodynamic properties such as temperature and flow rates with a satisfying accuracy (maximum mean deviation of 20% when predicting thermal resistances). However, please note that because the proposed adjustments were only performed on a given case (one heat exchanger configuration), the actual validity of the adjusted correlation on a larger domain is unknown.

Further possible improvements, both to the model and to the thermosyphon loop are described.

Declaration of competing interest

The authors declare that they have no known competing financial interests or personal relationships that could have appeared to influence the work reported in this paper.

Acknowledgment

This work was supported by a grant overseen by the French National Research Agency (ANR) as part of the “Investissements d’Avenir” Program ANE-ITE-002-01.

References

- [1] M. Cooper, Heat flow rates in saturated nucleate pool boiling—a wide-ranging examination using reduced properties, in: *Advances in Heat Transfer*, Vol. 16, Elsevier, 1984, pp. 157–239.
- [2] H. Louahlia-Gualous, S. Le Masson, A. Chahed, An experimental study of evaporation and condensation heat transfer coefficients for looped thermosyphon, *Appl. Therm. Eng.* 110 (2017) 931–940.
- [3] J. Millán, P. Godignon, X. Perpiñà, A. Pérez-Tomás, J. Rebollo, A survey of wide bandgap power semiconductor devices, *IEEE Trans. Power Electron.* 29 (5) (2014) 2155–2163.
- [4] H. Reynes, J. Maneiro, C. Buttay, P. Dworakowski, Thermal management optimization of a 5 MW power electronic converter, in: *12th European Advanced Technology Workshop on Micropackaging and Thermal Management, IMAPS, La Rochelle, France, 2017*.
- [5] J.-Y. Jung, H.-S. Oh, D.K. Lee, K.B. Choi, S.K. Dong, H.-Y. Kwak, A capillary-pumped loop (CPL) with microcone-shaped capillary structure for cooling electronic devices, *J. Micromech. Microeng.* 18 (1) (2007) 017002.
- [6] A. Chehade, H. Louahlia-Gualous, S. Le Masson, E. Lépinasse, Experimental investigations and modeling of a loop thermosyphon for cooling with zero electrical consumption, *Appl. Therm. Eng.* 87 (2015) 559–573.
- [7] K. Smith, G. Byrne, R. Kempers, A. Robinson, Electrohydrodynamic augmentation of a reflux thermosyphon, *Exp. Therm. Fluid Sci.* 79 (2016) 175–186.
- [8] A.H. Mayer, *Magnetic Two-Phase Thermosyphon*, Google Patents, 1983, US Patent 4, 366, 857.
- [9] D. Reay, R. McGlen, P. Kew, *Heat Pipes: Theory, Design and Applications*, Butterworth-Heinemann, 2013.
- [10] J. Cao, Z. Zheng, M. Asim, M. Hu, Q. Wang, Y. Su, G. Pei, M.K. Leung, A review on independent and integrated/coupled two-phase loop thermosyphons, *Appl. Energy* 280 (2020) 115885, <http://dx.doi.org/10.1016/j.apenergy.2020.115885>, URL <https://www.sciencedirect.com/science/article/pii/S0306261920313568>.
- [11] T. Ding, X. Chen, H. Cao, Z. He, J. Wang, Z. Li, Principles of loop thermosyphon and its application in data center cooling systems: A review, *Renew. Sustain. Energy Rev.* 150 (2021) 111389, <http://dx.doi.org/10.1016/j.rser.2021.111389>, URL <https://www.sciencedirect.com/science/article/pii/S1364032121006742>.
- [12] S. Zou, Q. Zhang, C. Yue, S. Du, Effect of servers’ arrangement on the performance of a loop thermosyphon system used in data center, *Appl. Therm. Eng.* 192 (2021) 116955, <http://dx.doi.org/10.1016/j.applthermaleng.2021.116955>, URL <https://www.sciencedirect.com/science/article/pii/S1359431121004026>.

- [13] C.J. Kim, B.O. Yoo, Y.J. Park, An experimental study of a two-phase closed loop thermosyphon with dual evaporator in parallel arrangement, *J. Mech. Sci. Technol.* 19 (1) (2005) 189–198.
- [14] D. Khrustalev, Loop thermosyphons for cooling of electronics, in: Eighteenth Annual IEEE Semiconductor Thermal Measurement and Management Symposium. Proceedings 2002 (Cat. No. 02CH37311), IEEE, 2002, pp. 145–150.
- [15] J.R. Hartenstine, R.W. Bonner III, J.R. Montgomery, T. Semenic, LOOP thermosyphon design for cooling of large area, high heat flux sources, in: International Electronic Packaging Technical Conference and Exhibition, 42770, 2007, pp. 715–722.
- [16] F. Agostini, B. Agostini, Flexible two-phase thermosyphon for power electronic cooling, in: 2011 IEEE 33rd International Telecommunications Energy Conference (INTELEC), IEEE, 2011, pp. 1–6.
- [17] T. Sukchana, N. Pratinthong, Effect of bending position on heat transfer performance of R-134a two-phase close loop thermosyphon with an adiabatic section using flexible hoses, *Int. J. Heat Mass Transfer* 114 (2017) 527–535, <http://dx.doi.org/10.1016/j.ijheatmasstransfer.2017.05.133>, URL <https://www.sciencedirect.com/science/article/pii/S0017931016339436>.
- [18] M. Moustaid, C. Buttay, V. Platel, Design considerations for the 2-phase cooling system of a 5 MW MVDC converter, in: 13th ATW European Workshop on Micropackaging and Thermal Management, La Rochelle, France, 2018.
- [19] 3M Electronics Markets Materials Division, Product Information, Tech. rep., 3M, 3M Center, Building 224-3N-11St. Paul, MN 55144-1000, 2009.
- [20] E. Forrest, J. Buongiorno, T. McKrell, L.-W. Hu, Pool boiling performance of Novec TM 649 engineered fluid, in: ECI International Conference on Boiling Heat Transfer, Florianopolis, Brazil, 2009.
- [21] D.J. Kearney, O. Suleman, J. Griffin, G. Mavrakakis, Thermal performance of a PCB embedded pulsating heat pipe for power electronics applications, *Appl. Therm. Eng.* 98 (2016) 798–809, <http://dx.doi.org/10.1016/j.applthermaleng.2015.11.123>, URL <https://www.sciencedirect.com/science/article/pii/S1359431115013848>.
- [22] B. Agostini, E. Ferreira, Nonintrusive measurement of the mass flow rate inside a closed loop two-phase thermosyphon, *Heat Pipe Sci. Technol. Int. J.* 2 (1–4) (2011) 1–12.
- [23] R. Dobson, J. Ruppertsberg, Flow and heat transfer in a closed loop thermosyphon. Part I—theoretical simulation, *J. Energy South. Afr.* 18 (4) (2007) 32–40.
- [24] M.E. Moustaid, V. Platel, C. Buttay, Study of convective condensation in a thermosiphon loop, in: 14th International Conference on Heat Transfer, Fluid Mechanics and Thermodynamics (HEFAT 2019), Wicklow, Ireland, 2019, pp. 1–6.
- [25] A. Cavallini, D.D. Col, L. Doretto, M. Matkovic, L. Rossetto, C. Zilio, G. Censi, Condensation in horizontal smooth tubes: A new heat transfer model for heat exchanger design, *Heat Transf. Eng.* 27 (8) (2006) 31–38.
- [26] V. Guichet, S. Almahmoud, H. Jouhara, Nucleate pool boiling heat transfer in wickless heat pipes (two-phase closed thermosyphons): A critical review of correlations, *Therm. Sci. Eng. Prog.* 13 (2019) 100384, <http://dx.doi.org/10.1016/j.tsep.2019.100384>, URL <https://www.sciencedirect.com/science/article/pii/S2451904919302045>.
- [27] V. Guichet, H. Jouhara, Condensation, evaporation and boiling of falling films in wickless heat pipes (two-phase closed thermosyphons): A critical review of correlations, *Int. J. Thermo fluids* 1–2 (2020) 100001, <http://dx.doi.org/10.1016/j.ijft.2019.100001>, URL <https://www.sciencedirect.com/science/article/pii/S2666202719300011>.